Accepted Manuscript

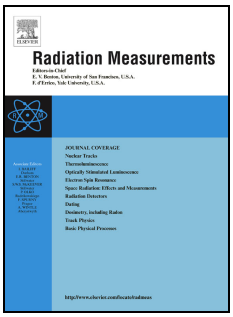

Title: The problem of dating quartz 1: Spectroscopic ionoluminescence of dose dependence

Authors: G.E. King, A.A. Finch, R.A.J. Robinson, D.E. Hole

PII: S1350-4487(10)00315-X

DOI: 10.1016/j.radmeas.2010.07.031

Reference: RM 4215

To appear in: *Radiation Measurements*

Received Date: 26 March 2010

Revised Date: 26 May 2010

Accepted Date: 30 July 2010

Please cite this article as: King, G.E., Finch, A.A., Robinson, R.A.J., Hole, D.E. The problem of dating quartz 1: Spectroscopic ionoluminescence of dose dependence, Radiation Measurements (2010), doi: 10.1016/j.radmeas.2010.07.031

The problem of dating quartz 1: spectroscopic ionoluminescence of dose dependence

G.E. King[a*], A.A. Finch[a], R.A.J. Robinson[a], D.E. Hole[b]

[a]School of Geography & Geosciences, University of St Andrews, Irvine Building, North Street, St Andrews, Fife, KY16 9AL, UK
[b]School of Engineering & Design, University of Sussex, Pevensey Building, Brighton, Sussex, BN1 9QH, UK
[*]corresponding author: georgina.king@gmail.com +44 (0)1334 463930

Abstract

A suite of quartz samples of different provenances, irradiation, thermal and depositional histories were analysed using spectroscopic ionoluminescence (IL) to investigate variations in emission spectra as a function of cumulative radiation dosing. Protons were selected for implantation to mimic the effect of natural radiation over geological timescales. All samples exhibited depletion in the UV-violet emission (3.2-3.4 eV) with increasing cumulative dose, whilst the red emission (1.8-1.9 eV) increased. A power-law relationship exists between the two emissions. It is inferred that the luminescence emission of quartz is indicative of its radiation history, and spectral analyses could be used to determine the utility of different quartz samples for optically stimulated luminescence dating (OSL) where the detection range is limited to 3.4-4.6 eV.

Keywords

Spectroscopic ionoluminescence, implantation, protons, quartz, optically stimulated luminescence dating.

Abbreviations

Ionoluminescence (IL), Ultra-violet (UV), Optically Stimulated Luminescence (OSL)

1. Introduction

OSL is used as a radiation dosimeter method within Quaternary geochronology, archaeology and retrospective accident dosimetry. Of the materials used for OSL studies, quartz is usually preferred (Aitken, 1998; Huntley et al., 1985). In addition, quartz has a range of industrial applications, which has rendered it the focus of intense research both into its physical and chemical properties, and its emission spectroscopy (see Götze, 2009; Krbetschek et al., 1997 for reviews). Numerous OSL dating applications to sediments of different ages (e.g. Ballarini et al., 2003; Pawley et al., 2008), provenances (e.g. Preusser et al., 2006) and depositional environments (e.g. Thrasher et al., 2009; Wallinga, 2002) have been made. However, despite the development of the single-aliquot regenerative dose protocol (Murray and Wintle, 2000), it is currently not possible to date all quartz using OSL. This is often due to quartz's highly variable OSL quantum efficiency (QE). The controls over quartz OSL QE remain unclear but have been linked to geological provenance (Götze et al., 2004; Rink et al., 1993; Westaway, 2009), irradiation (Rink, 1994), transport and thermal histories (Pietsch et al., 2008; Preusser et al., 2006). However quartz with the same irradiation, source and depositional histories often exhibit highly variable emission intensities (Duller et al., 2000; McFee and Tite, 1998).

The light emitted by quartz most commonly comprises bands in the UV-blue and red/IR (Krbetschek et al., 1997). Risø readers, the most widely used OSL instrumentation, stimulate the quartz with diodes at 470±20 nm (2.6 eV) and measure the response through Hoya U340 filters (Bøtter-Jensen et al., 2000). The transparency of these filters lies between 3.4 and 4.6 eV and only a part of the UV-blue emission band is monitored. The remainder of the emission (below 3.4 eV and above 4.6 eV) is unmeasured in conventional OSL but may contain significant dosimetry or geological provenance information.

Ionoluminescence (IL, also known as ion beam luminescence, IBL) is the study of light emitted from a sample when it is implanted with ions. By selecting specific ion species and implantation energy, ion-implantation can be applied at conditions equivalent to irradiation with ionising radiation. In the present study, we implant quartz with protons at 0.95 MV to explore the luminescence as a function of dose. This mimics the processes that occur in natural samples during irradiation over geological timescales, and allows the influence of radiation history, one of the proposed controls of quartz OSL QE, to be understood more fully. We compare and contrast our results with the luminescence spectra of natural quartz samples. Furthermore because IL involves high excitation energies, it is possible to examine the full UV-IR (6.2-1.1 eV) emission spectrum of quartz which provides a clearer indication of the complex quartz luminescence emission.

These experiments explore a number of hypotheses: 1. that quartz of different provenances exhibit different luminescence emission spectra; and 2. that radiation dosing promotes a change in the luminescence emission of quartz at both room temperature (RT) and liquid nitrogen (LNT) temperatures. Testing and accepting hypotheses 1 and 2 could help identify how trace elements influence luminescence centre behaviour, why quartz from certain geological histories have different emissions, and why dose history influences luminescence sensitivity. Hypothesis 3 is that the luminescence emission of quartz exhibits anisotropic effects. Unlike feldspar, quartz does not contain good cleavage, which results in a much greater range of probable orientations when multiple 180-250 µm grains are deposited onto discs. Therefore relative to their structure, there is a greater chance of random orientations occurring, making measurements of single grains more prone to anisotropic effects.

2. Materials and Methods

2.1 Samples

Calibration quartz (CalQz), from the Risø National Laboratory, Denmark, is used globally to calibrate both individual Risø reader machines and provide inter-laboratory comparisons (Buylaert et al., 2006). It has a very bright OSL signal, typically two orders of magnitude greater than the Scottish samples (WTUL1 and WTUL2: see below). Batch 8

CalQz is sedimentary quartz from Jutland, Denmark, which has been annealed at 500°C and dosed with 5.10 ± 0.06 Gy. It was prepared using conventional OSL methods at Risø and comprises 180-250 µm grains. Two Scottish samples (WTUL1 and WTUL2) are derived from Younger Dryas glacial outwash deposits, collected from a sediment exposure adjacent to the Water of Tulla, Central Highlands (56°34'N, -4°41'W). In December 2007 WTUL quartz samples were extracted from bulk material, following conventional OSL sample preparation involving desiccation, sieving to isolate the 180-212 µm grain size fraction, H_2O_2 treatment, density separation using 2.70 g cm^{-3} LST fastfloat, which is a heavy liquid comprising low toxicity sodium heteropolytungstates dissolved in water, and two 40 minute, 40 % HF etches prior to a final HCl wash. The quartz grain samples were mounted using UHU glue diluted with acetone, onto 10 mm^2 stainless steel discs (conventionally used for OSL dating) which were then mounted on an aluminium sheet and inserted into the sample chamber. We also analysed a natural hydrothermal quartz macrocrystal to explore response as a function of crystal orientation. Two 10 mm x 5 mm x 5 mm sections were cut parallel (QzPara) and perpendicular (QzPerp) to the *c*-axis and were finely polished. The quartz macrocrystal samples were mounted directly onto an aluminium sheet using UHU glue diluted with acetone. All errors are quoted at the 95 % confidence interval (2 σ).

2.2 Ionoluminescence

Ionoluminescence was performed under vacuum using the 3 MV van de Graaff particle accelerator at the University of Sussex following the methodology of Brooks et al. (2002). The ion-beam was focussed to a spot of 0.25 cm^2 and the IL of quartz was explored using H^+ ion species at an acceleration potential of 0.95 MV, with repeated 190 s exposures. The ion current was ~50 nA. Protons were selected because their low mass causes the least sample modification. Their behaviour can be very precisely modelled using packages such as SRIM (The Stopping and Range of Ions in Matter: Ziegler et al., 2008), which provide excellent constraint of energy dynamics during the interaction. SRIM modelling indicates that within these experiments, energy is transferred as electronic excitation over depths of ~11 µm.

Analyses were conducted at both room (RT=300 K) and liquid nitrogen temperatures (LNT=77 K). The sample was aligned at an angle of 22.5° to the incident beam, to enable emission collection at an angle of 45° relative to the excitation energy, and thus ensure maximum signal recording. Light emissions were collected by a quartz fibre optic coupled to a *f*/4 SpectroPro 300i monochromator. The detector used was a Roper Scientific image intensified CCD camera operated using the WinSpec software package. Experiments were conducted at RT with the exception of several spectra for QzPara and QzPerp collected at 77 K. The system operates between 1.1-6.2 eV using a coarse grating to perform two separate spectral analyses between 1.1-2.5 eV and 2.0-6.2 eV respectively. The two spectra were matched in the 2.0-2.5 eV region. Intensity data were normalised linearly for variations in the ion beam current. The spectra are corrected for background and system response against a W lamp by assuming a modified grey body radiation profile (Finch et al., 2004) using software written in house. Corrected spectra have then been converted to energy space through calculation of eV from wavelength, and by calculation of $I(E)dE$ from $I(\lambda)d\lambda$ by multiplication by $energy^2$ (Hamilton et al., 1978).

3. Results

3.1 Modelling of the Interaction by SRIM

The interaction of protons and quartz were modelled using TRIM (Transport of Ions in Matter), part of the SRIM package, through exploration of the interaction of 10^5 ions with a 180 µm thick quartz sample, density 2.66 g cm^{-3} (Fig. 1). TRIM calculates the amount of energy lost by the implantation ions to the target through ionization, phonon release and ion displacements at 0 K. Although the model does not account for temperature, which influences bond energies within the material, it is still useful for estimating the effects of

implantation. TRIM estimates that >99 % of the implantation energy is lost as ionization. The remaining <1 % energy loss is due to phonon production, predominantly from atom recoil. Few vacancies are produced due to the low mass of protons relative to oxygen or silicon atoms. TRIM indicates that ionization is concentrated at shallower depths (<10.8 µm) than phonon production. Luminescence is produced from the ionized region, and thus IL predominantly provides insights into the unaltered bulk of the sample, rather than the modified sample portion, which develops at the end of the ion track.

Figure One.

3.2 IL emission spectra and dose dependence

The initial IL emission spectra of the samples are given in Fig. 2. The alignment process and first integration time typically took 190 s and hence these spectra are the integral luminescence associated with the first ~4 x 10^7 Gy. The spectra comprise multiple emission bands, which can be deconvolved to comprise between 5 and 7 Gaussian components (Fig. 3). The fit of the model was tested using the X^2 parameter after Stevens-Kalceff (2009), whereby no further components were added once improvement in X^2 had stabilised.

Visual analysis of the emission spectra resulted in the identification of four different emissions at 1.8-1.9 eV (red), 2.6-2.7 eV (blue), 3.2-3.4 eV (UV-violet) and 3.6-6.7 eV (UV) (Fig. 2). Deconvolution indicated that the 1.8-1.9 eV emission is a composite of at least two emissions at 1.7-1.9 (red) and 2.0 eV (orange), and also revealed an additional emission at 1.4-1.5 eV (IR). All spectra are dominated by the red and UV-violet emissions, the energies of which vary between the different quartz,, with CalQz exhibiting peak emissions at 1.9 and 3.4 eV, QzPerp at 1.8 and 3.3 eV, and both WTUL samples at 1.8 and 3.2 eV. All samples with the exception of CalQz also exhibit a 3.7 eV emission, QzPerp exhibits a 2.6 eV emission and WTUL1 and WTUL2 a 2.7 eV emission. Due to difficulties with ion-beam stability, QzPara was irradiated during system alignment and the first spectrum recorded corresponds to 1.6 x 10^8 Gy implantation, thus it is excluded from Fig. 2.

Figure Two.
Figure Three.

The width of the filter conventionally used during OSL dating of quartz using a Risø reader is also shown in Fig. 2. The UV-blue emission is not entirely covered by the OSL detection window (3.4-4.6 eV) and just the tail of this emission is measured in OSL. CalQz has the most intense UV-violet relative to red emission of all of the samples analysed, whereas the UV-violet is much less pronounced in WTUL and QzPerp.

As proton implantation continues for all samples, the UV and UV-violet emission intensity reduces and the red emission increases in intensity. The UV-violet and red emissions also broaden (Fig. 4). The blue emission disappears from QzPerp, WTUL1 and WTUL2. The median red emission energy shifts from ~1.8 eV to ~1.7 eV in WTUL and from ~1.9 to ~1.85 eV in CalQz. These results on natural materials are similar to data reported from high-grade synthetic quartz (Bettiol et al., 1997). Although those authors recorded no UV emission, they did observe a single broad red emission at 660 nm (1.88 eV), which increased in intensity with increasing dose.

In order to determine whether the changes in the spectra were transitory or permanent, one sample (QzPerp) was left at RT for 15 hours, and the spectrum repeated. No recovery of the sample is observed, and thus we infer that these radiation dose effects are stable over timescales of days. This experiment also confirms that the modification of the IL is not just due to local thermal effects.

Figure Four.

3.3 Anisotropy of the Light emitted

Comparison of QzPara and QzPerp allows the anisotropy of luminescence to be determined. Analysis of the spectrum at 1.6 x 10^8 Gy shows that the relative amplitude of the red to the UV-violet emission is much greater for QzPara than for QzPerp (Fig 5.). After implantation with 2.3 x 10^8 Gy, the UV-violet emission was significantly reduced relative to the red in both samples, although both emissions were still present. IL was also measured at 77 K on fresh areas of QzPara and QzPerp (Fig. 6) and a single pronounced blue emission at 2.7 eV was recorded. This emission was apparent in QzPerp at RT, although was rapidly quenched by implantation. Counts for the intensity of the blue emission were an order of magnitude greater than for the UV-violet emission observed at RT. No spectra or intensity shift was observed for either QzPara or QzPerp when exposed as a function of dose at LNT, however there was some emission variability which may relate either to local sample warming or short (s) period fluctuations in the beam.

Figure Five.
Figure Six.

4. Discussion

4.1 Room Temperature IL

The origins of the luminescence emissions of quartz have been explored using contrasting spectroscopic techniques including cathodoluminescence, radioluminescence, photoluminescence and electron spin resonance (see Preusser et al., 2009; Stevens-Kalceff and Phillips, 1995 for a review). The RT (300 K) IL spectra are similar to those observed from quartz and silica glass by other authors (e.g. rose quartz: Kibar et al., 2007; silica glass: Kononenko et al., 2007) and are similar to quartz RL (Fujita and Hashimoto, 2006) and CL spectra (Götze et al., 2001; Stevens-Kalceff, 2009). Each excitation method differs energetically; for example, CL delivers energies of kV and excites only the surface region of the sample, whereas IL delivers MV but excites the sample bulk (Brooks et al., 2002; Townsend et al., 1999; Townsend and Rowlands, 2000). Despite these differences, useful insights into the emission properties of quartz can be obtained as the same centres are excited.

4.2 The UV-blue Emissions

Although some debate in its origin remains (e.g. McKeever, 1991; Yang and McKeever, 1990), it is widely assumed that the 380 nm (3.3 eV) UV-blue emission is associated with the substitution of Si^{4+} with Al^{3+}, charge compensated by protons or interstitial alkali ions (Alonso et al., 1983; Itoh and et al., 2002; Perny et al., 1992). This results in the formation of $[AlO_4/M^+]^\circ$ centres, where the Al^{3+} is charge compensated by either Li^+, Na^+ (Perny et al., 1992) or H^+ (Itoh and et al., 2002; Luff and Townsend, 1990). It should be noted that other entities such as Ge^{4+}, Ti^{4+} and H_3O_4 may also substitute for Si^{4+}, although such substitutions are less thermodynamically favoured and are dependent upon the crystallisation conditions (Götze et al., 2004). Similarly the abundance of the different charge-compensating alkali ions is also determined by the crystallisation conditions: e.g. Li^+ occurs in higher concentrations in pegmatitic quartz (Rink et al., 1993). The process of electron recombination at this centre is complex, and may reflect the development and decay of precursor centres (see Itoh and et al., 2002; McKeever, 1991; Yang and McKeever, 1990 for a discussion). The role of the interstitial alkali ions as charge carriers for the $[AlO_4/M^+]^\circ$ centres has been confirmed through comparison of 'swept' and 'unswept' quartz luminescence emissions, where the swept quartz has been exposed to intense electron irradiation in a hydrogen atmosphere, causing removal of alkali ions (Alonso et al., 1983; Martini et al., 1995). Swept quartz exhibited no UV emission at 380 nm (3.3 eV), in contrast to an unswept portion of the same sample. Furthermore, it has been inferred that this is the same centre accessed during OSL

through comparative OSL, TL, CL and ESR spectroscopies (Itoh and et al., 2002; Martini et al., 2009; Martini et al., 2000; Martini et al., 1995). We infer that the UV-violet IL in our samples comes from the same centre, as the emission energies are the same. This is consistent with our observation that CalQz exhibits the most intense IL UV-violet emission, in addition to the most intense OSL UV-blue emission. Martini et al. (1995) suggest that the population of $[AlO_4/M^+]^\circ$ centres is linked to low photon luminescence of quartz, thus we infer that CalQz must have an enhanced population of these centres relative to the other samples analysed.

The UV-violet emission modifies during implantation (Fig. 4), where depletion of the emission is observed, with increasing radiation dose. This dependence of the UV-violet emission to irradiation has also been observed (Botis et al., 2006; Krbetschek and Trautmann, 2000; Rink, 1994), although no precise mechanisms have been determined (Alonso et al., 1983; Halperin and Sucov, 1993; Itoh et al., 2002; Yang and McKeever, 1990). Exploration of the properties of the extrinsic $[AlO_4/M^+]^\circ$ defect using CL and ESR, has revealed that the population is highly sensitive to irradiation (Luff and Townsend, 1990; Perny et al., 1992; Weil, 1984). This can also be identified by the depletion of the signal with increasing exposure, as observed within our IL experiments (Fig. 4). This is attributed to the accelerated migration of the interstitial alkali ions (Halliburton et al., 1981), which are mobile along the c-axis of the quartz crystal at temperatures >200 K (Durrani et al., 1977; McKeever 1984; Stevens-Kalceff and Phillips, 1995). Furthermore radiation dosing has been identified as affecting the OSL and TL emissions of quartz, (Durrani et al., 1977; Hochman and Ypma, 1988; Levy, 1979; Rink, 1994). All of these observations are consistent with IL accessing the same centres observed by OSL and other spectroscopies.

UV-blue luminescence has also been attributed to other causes. Al^{3+} substituted for Si^{4+} can also be charge-compensated by a bridging electron hole, a centre given the annotation $[AlO_4]^\circ$ (Martini and Galli, 2007) and, in a clustered form, believed to contribute to the blue CL of feldspar (Finch and Klein, 1999). Such centres would be formed if the alkali ion were removed from $[AlO_4/M^+]^\circ$ centres and we would expect ion migration to shift luminescence between these two centre types. Second, UV-blue luminescence has been linked to oxygen vacancies in a variety of different guises, called the E'-centres (see Weil, 1984 for a review). In many cases, the vacancy can couple with other defects such as protons. These may produce UV-blue luminescence, or they may compete with UV-blue centres to dissipate energy non-radiatively (Poolton et al., 2000). The formation of E'-centres has been linked to irradiation, as oxygen vacancies are created (Durrani et al., 1977; McKeever 1984).

Understanding the dose dependence of IL provides insights into which of the above scenarios is most likely in these quartz samples. The interplay between $[AlO_4/M^+]^\circ$ and $[AlO_4]^\circ$ hinges on alkali and proton mobility during IL. Ion diffusion in quartz is believed to lie predominantly parallel to the c-axis as the structure has channels in this direction. Implantation would reduce the activation energy (Brooks et al., 2001) associated with hopping between adjacent channels. However, it is unclear from first principles whether such mobility would cause the motion of alkali metals away from $[AlO_4/M^+]^\circ$ centres to create $[AlO_4]^\circ$ centres or vice versa. The luminescence profile of the UV-violet region changes significantly during the implantation, in addition to the gross reduction of the overall UV-violet signal (Fig. 3). The UV-violet peak is initially at 3.3 eV but broadens progressively. Deconvolution indicates that the UV-violet band comprises at least two components at 3.3 and ~3.6 eV and that implantation modifies the relative proportions of these two components. If we accept that the 3.3 eV emission results from $[AlO_4/M^+]^\circ$ (Alonso et al., 1983; Itoh et al., 2002; Perny et al., 1992), we can suggest that the 3.6 eV centre is from $[AlO_4]^\circ$ and that ion migration during implantation is away from the centre. QzPara and QzPerp exhibit UV emissions at 3.6-3.7 eV before significant implantation. Only a small amount of literature has been published about the origins of this emission, however it has been attributed to the recombination of electrons at oxygen vacancies (Itoh et al., 2002; Rink et al., 1993). Heavy ion implantation generates oxygen vacancies, but

the use of protons means that this is minimal (see section 3.1) and the few vacancies that are formed are at the end of the ion track. As this region contributes very little to the luminescence signal we do not consider oxygen vacancy formation to be a credible explanation for the substantial changes seen here. Similarly the formation of AlOH centres and $[H_3O_4]^o$ centres (Nuttall and Weil, 1980; Yang and McKeever, 1990) as a consequence of proton implantation will be concentrated in this region, and thus are also unable to explain the observed depletion of the UV-violet to the benefit of the red.

4.3 The Red Emission

All samples exhibit a red emission at 1.8-1.9 eV. Deconvolution indicated that this emission is a composite of at least two emissions at 1.7-1.8 eV and 2.0 eV, which are attributed to Fe^{3+} impurities and non-bridging oxygen hole centres (NBOHC) respectively. The substitution of Si^{4+} with tetrahedral Fe^{3+}, has been associated with emissions at 1.75 eV (Kempe et al., 1999; Pott and McNicol, 1971) and 1.65 eV (Stevens-Kalceff, 2009). Red-IR (1.7 eV) luminescence in feldspar, another framework silicate, has also been linked to tetrahedral Fe^{3+} using ESR (Finch and Klein, 1999). Red emissions at 1.88 eV have been related to a NBOHC, the concentration of which is dependent on precursor peroxy linkage and hydroxyl group populations (Bettiol et al., 1997; Götze, 2009; Stevens-Kalceff and Phillips, 1995).

In contrast to the UV-violet emission, the red emission exhibits an increase in luminescence intensity with increasing radiation dose. Similar observations have been reported previously for both CL and IL, and were interpreted as either due to development of NBOHC as peroxy linkages are broken and the radiolysis of hydroxyl groups occurs (Stevens-Kalceff and Phillips, 1995), or to the creation of oxygen vacancies throughout irradiation (Luff and Townsend, 1990; Stevens-Kalceff and Phillips, 1995).

Luff and Townsend (1990) observed dose dependent effects in quartz luminescence during electron irradiation (CL), whereby the 2.6 eV emission was quenched whilst the 1.9 eV emission increased in intensity throughout exposure. The sensitization in the orange-red emission was permanent. Bettiol et al. (1997) also observed similar emission modification throughout 3 MV proton–excited IL of a sample for ten minutes at 295 K, which they also attributed to formation of NBOHC.

4.4 Interrelationships between the UV-blue and red emissions

All of the samples have different ratios of the intensity of UV-violet to red light emission at the onset of the experiment. Variations in this ratio are indicative of the specific precursor defect populations in samples prior to irradiation, which are the product of their crystallisation history (Götze, 2009) and dose history. Despite differing initial ratios of red and UV-violet emissions, all of the samples exhibit reduction in the intensity of the UV-violet emission alongside enhancement of the red emission as a function of ion implantation. There are three ways in which to interpret the data. The interaction may:

1) reduce the population of those centres that give rise to UV-violet luminescence through one mechanism and create the red luminescent centres through another,
2) reduce the population of UV-violet centres and increase the population of red centres through a single mechanism, or
3) have no effect on the population of red centres, but by reducing the population of UV-violet centres, energy which would have previously been emitted from a UV-violet recombination site is able to cascade to the red luminescent recombination site.

We infer that the overall reduction in the UV-violet emission results from reductions in the populations of $[AlO_4/M^+]^\circ$ and $[AlO_4]^\circ$ type centres caused by ion and electron migration. The $[AlO_4]^\circ$ centre would be charged (-1) if it were not for the coupling of the Al defect with a paramagnetic oxygen hole centre, effectively a coupled NBOHC. Our data are consistent with a mechanism in which ion and electron migration causes a change in the centre types from:

$[AlO_4/M^+]^\circ$ >> $[AlO_4]^\circ$ + $M^+_{(free)}$ >> $[AlO_4]^-$ + $NBOHC_{(free)}$

Luminescence: 3.3 eV 3.6 eV 1.9 eV

Such an interpretation implies that the increase in the red luminescence represents increasing the population of NBOHC and does not call upon oxygen vacancy formation, in accordance with our TRIM model results. To understand this further, we have examined the luminescence dose dependence of the UV-violet/red ratio. The dose dependence exhibits an exponential relationship (Fig. 7), the gradient of which is negative and ranges from -2.08 ± 1.19 for QzPara, to 1.14 ± 0.13 for WTUL2, which have the steepest and most shallow slopes respectively (Table 1). The power dependencies of all samples overlap within errors, and where QzPara is excluded, the average slope is -1.12 ± 0.11. Exclusion of QzPara is justified due to its greater implantation throughout experimentation (see section 3.2). We consider the consistency of the slopes in these graphs to indicate that, whatever the mechanism, it is the same process occurring in all the quartz samples studied. On average we determine the dose dependence of quartz to be governed by the relationship:

$$\frac{I_{UV-violet}}{I_{red}} = Ae^{-1.12D}$$

Where $I_{UV\text{-}violet}$ is the emission count at 3.26 eV, and I_{red} the emission count at 1.9 eV, which are the average central values for the UV-violet and red composite emissions identified visually for the different quartz samples. D is the dose (Gy) and A represents different initial ratios of the UV-violet and red luminescence. The pre exponential factor A is within error for all samples, ranging from 7.64 ± 0.93 for WTUL1 and 8.43 ± 1.22 for CalQz where QzPara is excluded. The annealing treatment that CalQz has received is known to increase OSL QE. One mechanism through which this could be achieved is the recovery of $[AlO_4/M^+]^\circ$centres through thermally induced remobilisation of alkali ions. The brighter luminescence of CalQz is thus reflected in its larger A value.

The slope of fig. 7 is not significantly different to 1. If the power dependence had been significantly greater or less than 1, we would have been able to infer that the rate of formation of red luminescence was significantly different to that of the reduction of the UV-violet light. As it is, we conclude that the rate of generation of quanta of red luminescence parallels within error the depletion in quanta of UV-violet. This is consistent with the model of NBOHC formation presented above. However it is also consistent with a model whereby reduction of the populations of UV-violet luminescent centres allows energy that would have been emitted at one of these centres to cascade further to the red luminescence centre. Such a model does not involve changes in the luminescence centre populations, rather that these are now accessible to the excited energy. If we accept the latter model, then luminescence from Fe^{3+} centres (Kempe et al., 1999; Pott and McNicol, 1971; Stevens-Kalceff, 2009) may indeed be the cause of the red luminescence, perhaps also associated with NBOHC formation. The contributions to red luminescence from these two types of centre may, in due course, be deconvolved by time-resolved luminescence spectroscopies.

Figure Seven.
Table One.

4.5 Dose Rate effects

Dose rate effects are problematic in all luminescence investigations, since laboratory experiments are completed over timescales that are geologically 'instantaneous'. We have considered whether dose rate, rather than integral dose, brings about the changes we observe. Brooks et al. (2001) contrasted IL from H^+ implantation with that of H_2^+ ions for sapphire. The H_2^+ ions dissociate on entering the sample to form separate excitation tracks which overlap both spatially and temporally. Such comparisons double the dose rate whilst all other conditions, notably the incident power, are kept constant. Brooks et al. (2001) recorded no dose rate effects. This is also consistent with Fujita and Hashimoto (2006) who explored the dose rate dependence of the RL of quartz. During sample dosing at RT, they also observed a strong RL emission at 3.1 eV for a range of dose rates from 0.1 to 10 Gys^{-1}. The RL emission intensity did not vary with dose rate. The total cumulative dose varied throughout our IL analyses whereas the dose rate remained approximately constant, thus we tentatively conclude that the observed luminescence emissions changes are an effect of cumulative dose rather than dose rate.

4.6 LNT IL Spectra

The 2.7 eV emission observed for all samples at LNT (Fig. 6) coincides with the 2.8 eV emission observed during low temperature CL of quartz (Itoh et al., 1989; Luff and Townsend, 1990) and IL of rose quartz (Kibar et al., 2007). It is an order of magnitude more intense than the RT spectrum, in agreement with Itoh et al. (1989), Luff and Townsend (1990) and Kibar et al. (2007). However, Bettiol et al. (1997) did not observe this emission peak when performing IL at 80 K on synthetic quartz, although the 1.88 and 2.3 eV emissions were enhanced.

Numerous origins for the 2.7 eV emission have been proposed. It may originate from an intrinsic oxygen-vacancy defect, attributed to the self-trapped exciton (Itoh et al., 1989; Itoh et al., 2002). It has been associated with E'-centre annihilation in glass (Sigel, 1973), although non-linearity in this relationship is indicative of some non-radiative E'-centre recombination in quartz (see McKeever 1984 for a review; Poolton et al., 2000). Alternatively it may be associated with the $[AlO_4/M^+]^\circ$ defect that produces the UV-violet emission at RT (Stevens-Kalceff and Phillips, 1995). This is regarded as the most plausible explanation as alkali ions are unable to diffuse through the crystal lattice at temperatures <200 K, which renders the centre insensitive to radiation exposure at LNT. No dose dependence was observed in either sample, following exposure to 1.25 x 10^8 Gy and 6.08 x 10^7 Gy for QzPara and QzPerp respectively.

4.7 Anisotropic Effects

The emissions of both QzPara and QzPerp were similar at LNT, both being dominated by the intense 2.7 eV emission, although QzPara exhibits a slightly stronger luminescence signal. At RT following exposure to 1.6 x 10^8 Gy, the UV-violet signal has depleted dramatically in both samples (Fig. 5), although the 3.2-3.3 eV and 3.6-3.7 eV emissions are still visible. QzPara exhibits the most intense red (1.9 eV) luminescence signal, whereas QzPerp exhibits the most intense UV-violet (3.2-3.3 and 3.6-3.7 eV) luminescence signal. These results indicate that grains aligned perpendicular to their *c*-axis will luminesce most brightly overall and in the red, however those aligned parallel to their *c*-axis will emit most brightly in the UV-violet.

5. Conclusions

The exposure of quartz to ion implantation results in an increasing red emission and decreasing UV-violet emission, the latter of which is conventionally used in OSL dating. This is consistent with irradiation-induced migration of charge compensating alkali ions from $[AlO_4/M^+]^\circ$ centres, which are considered responsible for the 3.3 eV UV-violet emission. The red emission may be enhanced through development of NBOHC as a direct consequence of irradiation, coupled with an increased availability of energy both at these centres and at Fe^{3+} centres. The dose dependence behaviour of all samples overlaps

within error. Variability between samples may relate to differences in provenance, specifically crystallisation environment and geological irradiation history, or alternatively to anisotropic effects.

Spectroscopic profiling using excitation methods such as IL, CL or RL provide valuable insights regarding which samples are likely to be suitable for OSL dating. These experiments provide an explanation for the observation that recently eroded quartz has poor luminescence sensitivity. If quartz is derived from relatively radioactive bedrock, such as granite, the UV-blue luminescence emission will already have been quenched. Thus their poor luminescence sensitivity is explained by their immediate, geologically determined, radiation history. Conversely the observation that highly weathered quartz which have undergone many cycles of deposition and transport have good OSL properties, can be explained as exposure to high temperatures or mechanical processes during transport may enable remigration of the alkali ions to their charge compensating interstitial locations, resulting in $[AlO_4/M^+]^\circ$ centre formation and UV-blue emission recovery.

Spectroscopic analyses of quartz luminescence emission are valuable in informing sample selection and analytical protocols, and should be utilised within OSL dating (Krbetschek et al., 1997; Townsend et al., 1993). These would enable identification of quartz likely to respond well in OSL analyses and may facilitate protocol development for more challenging samples.

Acknowledgements

GEK was supported by NERC studentship F008589/1, and would like to thank the Mineral Physics Group of the Mineralogical Society of Great Britain and Ireland for a travel grant, which enabled presentation of this research at LED 2008. Special thanks are also given to Henrik Friis who assisted with data collection as well as to two anonymous reviewers whose comments improved the manuscript significantly.

Figure 1: TRIM model of 10^5 protons at 0.95 MV implanting quartz 180 µm thick, density 2.66 g cm^{-3} (Ziegler et al., 2008). The upper graph predicts the pathway of incident ions, indicating clustering over ~9 µm and that maximum sample penetration is ~11 µm. The middle graph indicates ion derived ionization peaks at 10.8 µm which accounts for > 2 orders of magnitude more energy dissipation than recoil derived ionization or phonon production, which both peak at 11.3 µm. The lower graph indicates that recoil production is low, and is clustered at ~11 µm depth.

Figure 2: Initial IL spectra obtained from each of the samples at RT. Data are plotted in energy space and have not been scaled for intensity (see text for details). Spectrum A: CalQz, B: WTUL2, C: WTUL1, D: QzPerp. The initial spectra comprise two main emission peaks at 1.8-1.9 eV and 3.2-3.4 eV. The conventional OSL detection window (3.4-4.6 eV), where Hoya U-340 filters are used is indicated (Ballarini et al., 2005).

Figure 3: Deconvolution of the initial CalQz emission spectra in energy space using multiple Gaussian components which indicate that the UV-violet and red emissions which dominate all samples, are composites of at least two emission centres.

Figure 4: Modification of the CalQz emission spectrum as a function of cumulative implantation dose (Gy). The initial spectrum is shown at the bottom of the figure.

Figure 5: QzPara and QzPerp emission spectra at RT following 1.6 x 10^8 Gy radiation dosing. The 3.2-3.4 eV UV-violet emission is highly amorphized in QzPerp, and is indistinct in QzPara, these emissions are shown at x 10 magnification in the inset. QzPara and QzPerp exhibit small 3.6 eV and 3.7 eV UV emissions respectively.

Figure 6: QzPara and QzPerp emission spectra at 77 K. The 1.8, 3.2 and 3.6-3.7 eV emissions at room temperature are replaced with an intense blue 2.7 eV emission. This emission is an order of magnitude brighter than the room temperature spectra.

Figure 7: A log-log plot of luminescence intensity versus dose. The UV-violet/red (filled diamonds) ratios are plotted relative to the second (right) y-axis, and are fitted with a power-law trendline (in log-log space). The UV-blue emission (open diamonds) exhibits reducing intensity with increasing dose, in opposition to the red emission (filled triangles). The bracketed data point on the QzPerp plot has not been included in calculation of the trendline, but is shown here in the interest of transparency.

References

Aitken, M.J., 1998. An Introduction to Optical Dating - the Dating of Quaternary Sediments by the Use of Photon-Stimulated Luminescence. Oxford Science Publications, Oxford.
Alonso, P.J., Halliburton, L.E., Kohnke, E.E., Bossoli, R.B., 1983. X-ray-induced luminescence in crystalline SiO[sub 2]. Journal of Applied Physics 54, 5369-5375.
Ballarini, M., Wallinga, J., Duller, G.A.T., Brouwer, J.C., Bos, A.J.J., Van Eijk, C.W.E., 2005. Optimizing detection filters for single-grain optical dating of quartz. Radiation Measurements 40, 5-12.
Ballarini, M., Wallinga, J., Murray, A.S., van Heteren, S., Oost, A.P., Bos, A.J.J., van Eijk, C.W.E., 2003. Optical dating of young coastal dunes on a decadal time scale. Quaternary Science Reviews 22, 1011-1017.
Bettiol, A.A., Nugent, K.W., Jamieson, D.N., 1997. The characterisation of high-grade synthetic quartz, corundum and spinel using ionoluminescence (IL). Nuclear Instruments and Methods in Physics Research Section B: Beam Interactions with Materials and Atoms 130, 734-739.
Botis, S., Pan, Y., Bonli, T., Xu, Y., Zhang, A., Nokhrin, S., Sopuck, V., 2006. Natural radiation-induced damage in Quartz. II. Distribution and implications for Uranium mineralization in the Athabasca basin, Saskatchewan, Canada. Can Mineral 44, 1387-1402.
Bøtter-Jensen, L., Bulur, E., Duller, G.A.T., Murray, A.S., 2000. Advances in luminescence instrument systems. Radiation Measurements 32, 523-528.
Brooks, R.J., Hole, D.E., Townsend, P.D., 2002. Ion beam induced luminescence of materials. Nuclear Instruments and Methods in Physics Research Section B: Beam Interactions with Materials and Atoms 190, 136-140.
Brooks, R.J., Ramachandran, V., Hole, D.E., Townsend, P.D., 2001. Dose rate effects in ion beam luminescence. Radiation Effects and Defects in Solids: Incorporating Plasma Science and Plasma Technology 155, 177 - 181.
Buylaert, J., Ankjaergaard, C., Murray, A.S., Nielsen, A., 2006. A proposed laboratory intercomparison sample based on a beach-ridge sand from Skagen (Denmark), UK Luminescence and ESR Meeting, Liverpool, UK.
Duller, G.A.T., Bøtter-Jensen, L., Murray, A.S., 2000. Optical dating of single sand-sized grains of quartz: sources of variability. Radiation Measurements 32, 453-457.
Durrani, S.A., Khazal, K.A.R., McKeever, S.W.S., Riley, R.J., 1977. Studies of changes in the thermoluminescence sensitivity in quartz induced by proton and gamma irradiations. Radiation Effects and Defects in Solids: Incorporating Plasma Science and Plasma Technology 33, 237 - 244.
Finch, A.A., Garcia-Guinea, J., Hole, D.E., Townsend, P.D., Hanchar, J.M., 2004. Ionoluminescence of zircon: rare earth emissions and radiation damage. Journal of Physics D: Applied Physics 37, 2795.
Finch, A.A., Klein, J., 1999. The causes and petrological significance of cathodoluminescence emissions from alkali feldspars. Contributions to Mineralogy and Petrology 135, 234-243.
Fujita, H., Hashimoto, T., 2006. Influence of Radioluminescence on Optically Stimulated Luminescence from Natural Quartz grains. Radioisotopes 55, 117-123.
Götze, J., 2009. Chemistry, textures and physical properties of quartz - geological interpretation and technical application. Mineral Mag 73, 645-671.
Götze, J., Plötze, M., Graupner, T., Hallbauer, D.K., Bray, C.J., 2004. Trace element incorporation into quartz: A combined study by ICP-MS, electron spin resonance, cathodoluminescence, capillary ion analysis, and gas chromatography. Geochimica et Cosmochimica Acta 68, 3741-3759.
Götze, J., Plötze, M., Habermann, D., 2001. Origin, spectral characteristics and practical applications of the cathodoluminescence (CL) of quartz – a review. Mineralogy and Petrology 71, 225-250.
Halperin, A., Sucov, E.W., 1993. Temperature dependence of the X-ray induced luminescence of Al-Na-containing quartz crystals. Journal of Physics and Chemistry of Solids 54, 43-50.
Hamilton, T.D.S., Munro, I.H., Walker, G., 1978. Luminescence Instrumentation, in: Lumb, M.D. (Ed.), Luminescence Spectroscopy. Academic Press, London, pp. 149-238.

Hochman, M.B.M., Ypma, P.J.M., 1988. Changes in the artificial thermoluminescence glow curves of quartz associated with uranium deposits. International Journal of Radiation Applications and Instrumentation. Part D. Nuclear Tracks and Radiation Measurements 14, 105-111.
Huntley, D.J., Godfrey-Smith, D.I., Thewalt, M.L.W., 1985. Optical dating of sediments. Nature 313, 105-107.
Itoh, et al., 2002. Ionic and electronic processes in quartz:Mechanisms of thermoluminescence and optically stimulated luminescence. Journal of Applied Physics 92, 5036.
Itoh, C., Tanimura, K., Itoh, N., Itoh, M., 1989. Threshold energy for photogeneration of self-trapped excitons in SiO2. Physical Review B 39, 11183.
Itoh, N., Stoneham, D., Stoneham, A.M., 2002. Ionic and electronic processes in quartz:Mechanisms of thermoluminescence and optically stimulated luminescence. Journal of Applied Physics 92, 5036-5044.
Kempe, U., Goetze, J., Dandar, S., Habermann, D., 1999. Magmatic and metasomatic processes during formation of the Nb-Zr-REE deposits Khaldzan Buregte and Tsakhir (Mongolian Altai); indications from a combined CL-SEM study. Mineral Mag 63, 165-177.
Kibar, R., Garcia-Guinea, J., Çetin, A., Selvi, S., Karal, T., Can, N., 2007. Luminescent, optical and color properties of natural rose quartz. Radiation Measurements 42, 1610-1617.
Kononenko, S.I., Kalantaryan, O.V., Muratov, V.I., Zhurenko, V.P., 2007. Silica luminescence induced by fast light ions. Radiation Measurements 42, 751-754.
Krbetschek, M.R., Götze, J., Dietrich, A., Trautmann, T., 1997. Spectral information from minerals relevant for luminescence dating. Radiation Measurements 27, 695-748.
Krbetschek, M.R., Trautmann, T., 2000. A spectral radioluminescence study for dating and dosimetry. Radiation Measurements 32, 853-857.
Levy, P., 1979. Thermoluminescence studies having application to geology and archaeology. PACT 3, 466-480.
Luff, B.J., Townsend, P.D., 1990. Cathodoluminescence of synthetic quartz. Journal of Physics: Condensed Matter 2, 8089-8097.
Martini, M., Fasoli, M., Galli, A., 2009. Quartz OSL emission spectra and the role of [AlO4]° recombination centres. Radiation Measurements 44, 458-461.
Martini, M., Galli, A., 2007. Ionic mechanisms in the optically stimulated luminescence of quartz. physica status solidi (c) 4, 1000-1003.
Martini, M., Meinardi, F., Vedda, A., 2000. The role of alkali ions in the 190 K TSL peak in quartz. Radiation Measurements 32, 673-677.
Martini, M., Paleari, A., Spinolo, G., Vedda, A., 1995. Role of [AlO_{4}]^{0} centers in the 380-nm thermoluminescence of quartz. Physical Review B 52, 138.
McFee, C.J., Tite, M.S., 1998. The detection of insufficiently bleached grains using an imaging photon detector. Archaeometry 40, 153-168.
McKeever , S.W.S., 1984. Thermoluminescence in Quartz and Silica. Radiation Protection Dosimetry 8, 81-98.
McKeever, S.W.S., 1991. Mechanisms of thermoluminescence production: Some problems and a few answers? International Journal of Radiation Applications and Instrumentation. Part D. Nuclear Tracks and Radiation Measurements 18, 5-12.
Murray, A.S., Wintle, A.G., 2000. Luminescence dating of quartz using an improved single-aliquot regenerative-dose protocol. Radiation Measurements 32, 57-73.
Nuttall, R.H.D., Weil, J.A., 1980. Two hydrogenic trapped-hole species in [alpha]-quartz. Solid State Communications 33, 99-102.
Pawley, S.M., Bailey, R.M., Rose, J., Moorlock, B.S.P., Hamblin, R.J.O., Booth, S.J., Lee, J.R., 2008. Age limits on Middle Pleistocene glacial sediments from OSL dating, north Norfolk, UK. Quaternary Science Reviews 27, 1363-1377.
Perny, B., Eberhardt, P., Ramseyer, K., Mullis, J., Panrath, R., 1992. Microdistribution of Al, Li, and Na in α quartz: Possible causes and correlation with short-lived cathodoluminescence. American Mineralogist 77, 535-544.
Pietsch, T.J., Olley, J.M., Nanson, G.C., 2008. Fluvial transport as a natural luminescence sensitiser of quartz. Quaternary Geochronology 3, 365-376.

Poolton, N.R.J., Smith, G.M., Riedi, P.C., Bulur, E., Bøtter-Jensen, L., Murray, A.S., Adrian, M., 2000. Luminescence sensitivity changes in natural quartz induced by high temperature annealing: a high frequency EPR and OSL study. Journal of Physics D: Applied Physics 33, 1007-1017.
Pott, G.T., McNicol, B.D., 1971. Spectroscopic study of the coordination and valence of Fe and Mn ions in and on the surface of aluminas and silicas. Discussions of the Faraday Society 52, 121-131.
Preusser, F., Chithambo, M.L., Götte, T., Martini, M., Ramseyer, K., Sendezera, E.J., Susino, G.J., Wintle, A.G., 2009. Quartz as a natural luminescence dosimeter. Earth-Science Reviews 97, 184-214.
Preusser, F., Ramseyer, K., Schlüchter, C., 2006. Characterisation of low OSL intensity quartz from the New Zealand Alps. Radiation Measurements 41, 871-877.
Rink, W.J., 1994. Billion-year age dependence of luminescence in granitic quartz. Radiation Measurements 23, 419-422.
Rink, W.J., Rendell, H., Marseglia, E.A., Luff, B.J., Townsend, P.D., 1993. Thermoluminescence spectra of igneous quartz and hydrothermal vein quartz. Physics and Chemistry of Minerals 20, 353-361.
Sigel, G.H., 1973. Ultraviolet Specta of Silicate Glasses: A Review of Some Experimental Evidence. Journal of Non-Crystalline Solids 13, 372-398.
Stevens-Kalceff, M.A., 2009. Cathodoluminescence microcharacterization of point defects in {alpha}-quartz. Mineral Mag 73, 585-605.
Stevens-Kalceff, M.A., Phillips, M.R., 1995. Cathodoluminescence microcharacterization of the defect structure of quartz. Physical Review B 52, 3122.
Thrasher, I.M., Mauz, B., Chiverrell, R.C., Lang, A., 2009. Luminescence dating of glaciofluvial deposits: A review. Earth-Science Reviews 97, 145-158.
Townsend, P.D., Karali, T., Rowlands, A.P., Smith, V.A., Vazquez, G., 1999. Recent examples of cathodoluminescence as a probe of surface structure and composition. Mineral Mag 63, 211-226.
Townsend, P.D., Rendell, H., Luff, B.J., 1993. High sensitivity TL spectra of quartz and feldspar. Ancient TL 11, 36-39.
Townsend, P.D., Rowlands, A.P., 2000. Information Encoded in Cathodoluminescence Emission Spectra, in: Pagel, M., Barbin, V., Blanc, P., Ohnenstetter, D. (Eds.), Cathodoluminescence in Geosciences. Springer-Verlag, Heidelberg, pp. 41-57.
Wallinga, J., 2002. Optically stimulated luminescence dating of fluvial deposits: a review. Boreas 31, 303-322.
Weil, J.A., 1984. A review of electron spin spectroscopy and its application to the study of paramagnetic defects in crystalline quartz. Physics and Chemistry of Minerals 10, 149-165.
Westaway, K.E., 2009. The red, white and blue of quartz luminescence: A comparison of De values derived for sediments from Australia and Indonesia using thermoluminescence and optically stimulated luminescence emissions. Radiation Measurements 44, 462-466.
Yang, X.H., McKeever, S.W.S., 1990. Point Defects and the Pre-Dose Effect in Quartz. Radiat Prot Dosimetry 33, 27-30.
Ziegler, J.F., Ziegler, M.D., Biersack, J.P., 2008. SRIM-20083.04: The stopping and range of ions in matter. SRIM.com.

Table 1: Dose Dependence and Pre-Exponential Terms for Implantation of Quartz.

Sample	Provenance	Log_{10} A	Power Dependence
CalQz	Risø Labs	8.4 ± 1.2	-1.11 ± 0.16
WTUL1	Glaciofluvial deposit	7.6 ± 0.9	-1.11 ± 0.11
WTUL2	Glaciofluvial deposit	8.2 ± 1.1	-1.14 ± 0.13
QzPara*	Hydrothermal	15.2 ± 9.9	-2.08 ± 1.19
QzPerp	Hydrothermal	7.8 ± 0.5	-1.11 ± 0.06

*The relatively large error for QzPara is due to its analysis with shorter acquisition periods (130 s), selected to minimise modification following its enhanced exposure during ion beam tuning.

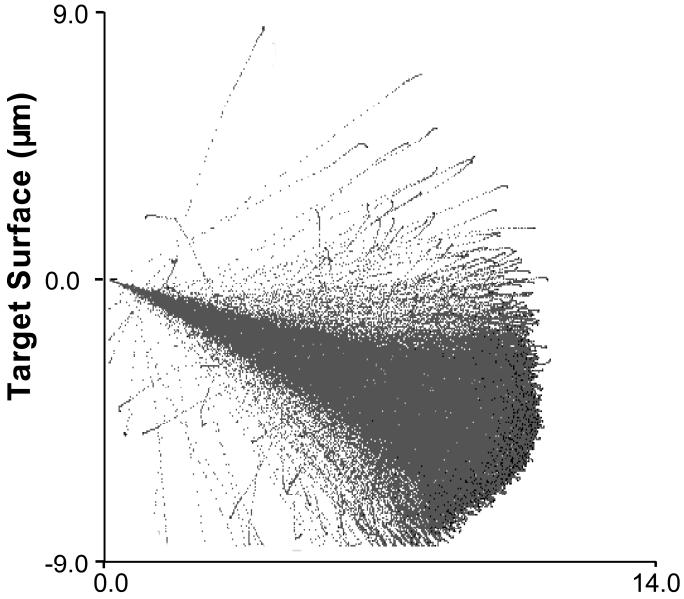

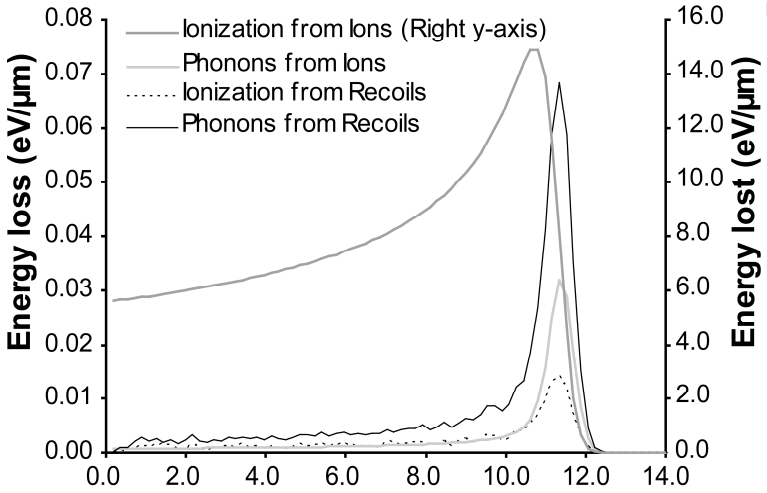

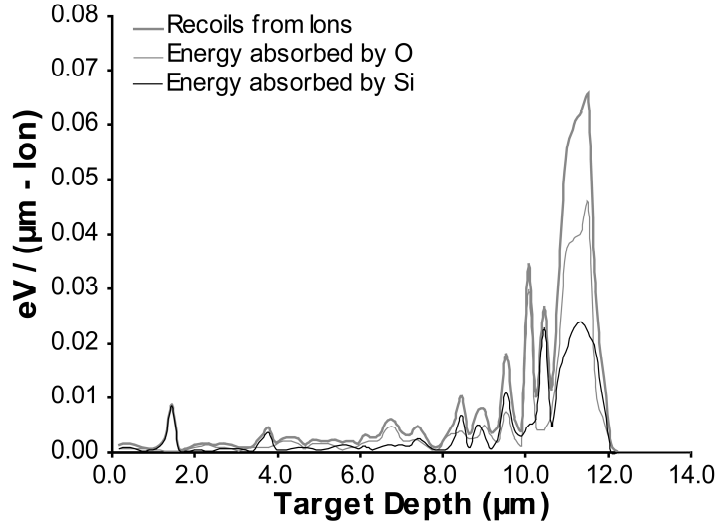

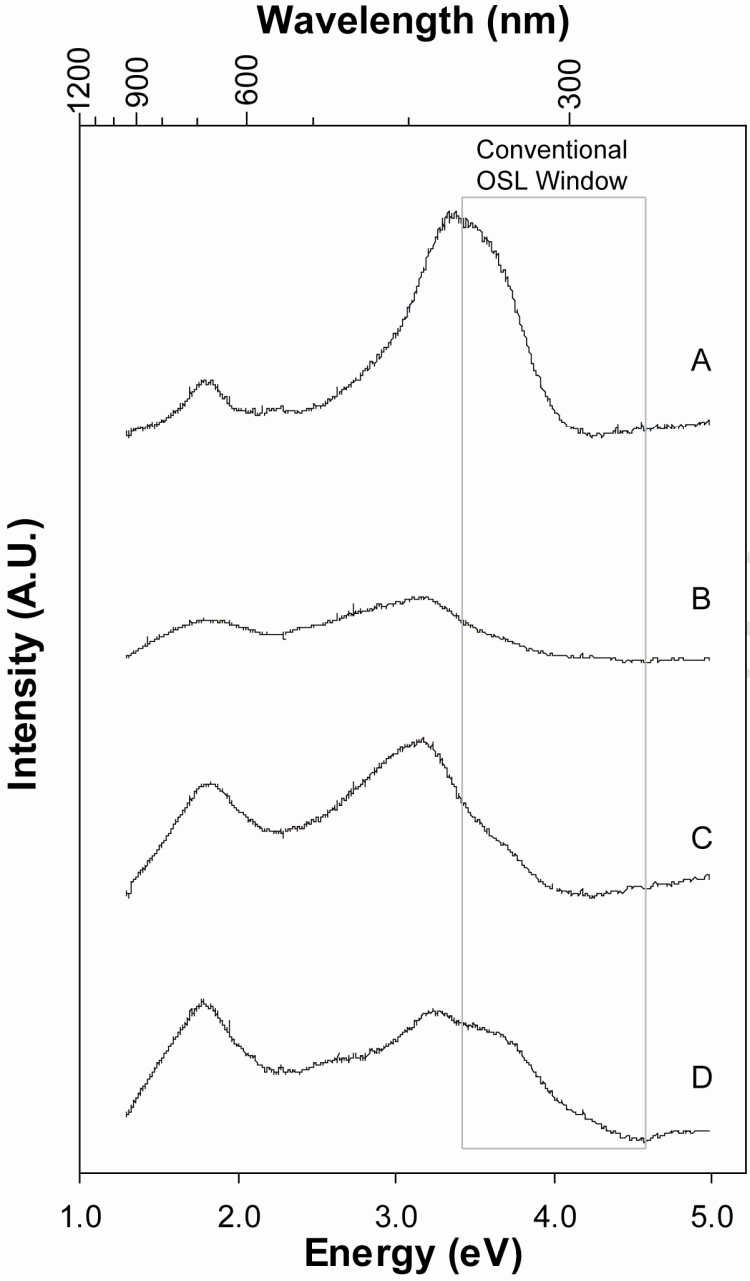

CalQz: Initial spectrum (2.08 x 10^7 Gy)

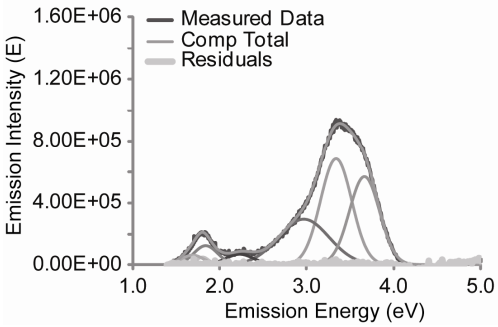

Component	mean (eV)	sigma (eV)	Intensity (E)	% Total Emission
1	3.66	0.17	5.67 x 10^5	32
2	3.34	0.18	6.82 x 10^5	38
3	2.97	0.29	2.92 x 10^5	16
4	2.23	0.16	7.21 x 10^4	4
5	1.84	0.14	1.22 x 10^5	7
6	1.69	0.13	6.20 x 10^4	3

Sum Squared Residuals: 6.57 x 10^{10}